

A method for detecting season-dependent modes of climate variability: S-EOF analysis

Bin Wang and Soon-Il An

International Pacific Research Center, School of Ocean and Earth Science and Technology, University of Hawai'i at Manoa, Honolulu, Hawaii, USA

Received 14 February 2005; revised 5 July 2005; accepted 18 July 2005; published 10 August 2005.

[1] Anomalous climate is often regulated by the annual cycle. Based on this physical consideration, we propose a new method termed as Season-reliant Empirical Orthogonal Function (S-EOF) analysis to detect major modes of climate variability. The S-EOF analysis of Indo-Pacific SST during the past 54 years reveals two statistically significant leading modes, which are not obtainable by using conventional EOF analysis. These modes represent the Indo-Pacific Low-Frequency (LF) and Quasi-Biennial (QB) modes associated ENSO, and reveal the fundamental differences between the LF and QB modes in their seasonal evolution, fractional variance structure, and interdecadal variation and trend. The interdecadal variability is coupled with the LF mode, suggesting that decadal-interdecadal SST variation is primarily represented by the ENSO-like interdecadal regime shift in the late 1970s. A warming trend is mingled with the QB mode, accounting for a large portion of the local SST variability in the Maritime Continent-western Pacific horseshoe region. **Citation:** Wang, B., and S.-I. An (2005), A method for detecting season-dependent modes of climate variability: S-EOF analysis, *Geophys. Res. Lett.*, 32, L15710, doi:10.1029/2005GL022709.

1. Introduction

[2] The EOF analysis decomposes spatial-temporal variations of a geophysical field into combination of orthogonal spatial patterns with corresponding principal components (PC) in a linear fashion [Lorenz, 1956]. It provides a powerful tool for identifying major modes of climate variability such as the El Niño/Southern Oscillation (ENSO) [Weare, 1982]. The EOF analysis, however, does not necessarily yield physically distinguished modes or help interpreting mechanisms. Figure 1 shows that the conventional EOF analysis of boreal winter (DJF) mean sea surface temperature (SST) anomalies in the Indo-Pacific Ocean yields only one leading mode that is statistically significant (distinguished from others) according to the rule of thumb by North *et al.* [1982]. This mode accounts for 39.3% of the total variance and represents a mature phase of ENSO. The corresponding PC consists of mixed temporal signals: low-frequency (LF) (4–5 years), quasi-biennial (QB) (2–3 years), and a long-term trend and interdecadal variations. Similar results are obtained when the summer (JJA) mean SST anomaly (SSTA) or all seasonal mean SSTA time series are analyzed (figure not shown). In all the three cases, the conventional EOF analysis yields a single, dominant mode

(mature phase of ENSO) with mixed multi-time scales ranging from biennial to interdecadal.

[3] Due to the difficulty of EOF analysis in distinguishing LF and QB components, the multi-faced ENSO behavior and the SST variability in the Indo-Pacific Ocean have to rely on usage of band-pass filtered data. The time filtering, however, is a subjective pre-processing approach. Can the two major components of ENSO (LF and QB) be objectively identified or separated without subject to prior time filtering? If so, one would have stronger confidence to seek for the fundamental differences between the LF and QB components of ENSO. Addressing this question is important for understanding the physics of SST variability and the behaviors of coupled ocean-atmospheric models, some of which have excessive biennial variations of simulated ENSO events.

[4] In the present paper, we put forward an objective approach, the Season-reliant EOF (S-EOF) analysis, for distinguishing modes of variability that evolve with season. We will demonstrate the usefulness of the S-EOF in identifying physically meaningful modes of SST variability and in revealing additional information for understanding of the nature of the LF and QB components of ENSO.

2. Methodology: The S-EOF Analysis

[5] Seasonal mean anomalies (departure from long-term mean annual cycle) are often the targets for climate analysis and prediction. The annual cycle of the coupled atmosphere-ocean-land system that is ultimately driven by solar irradiance variation plays an essential role in locking ENSO phase to the annual cycle [An and Wang, 2001] and in controlling chaotic ENSO dynamics [e.g., Wang and Fang, 1996]. Because the annual cycle is a pacesetter and regulator for interannual SST variations, our objective is to describe SST variability with emphasis on its seasonal-dependent evolution. A basic assumption behind the S-EOF is that interannual to interdecadal SST variability may be strongly modulated by the seasonal march of the solar radiation forcing and the resultant climatological annual cycles.

[6] The idea of S-EOF is illustrated in terms of analysis of the year-to-year variations of SSTA with special interest in the seasonally evolving pattern from one year to another. Rather than examining a single seasonal mean SSTA for each year or for all seasons, we now examine the SSTA in a seasonal sequence beginning from the winter of a year denoted as D(-1)JF(0) to the following fall SON(0), i.e. D(-1)JF(0), MAM(0), JJA(0), SON(0), where -1 denote the year before year 0, MAM and SON denotes boreal

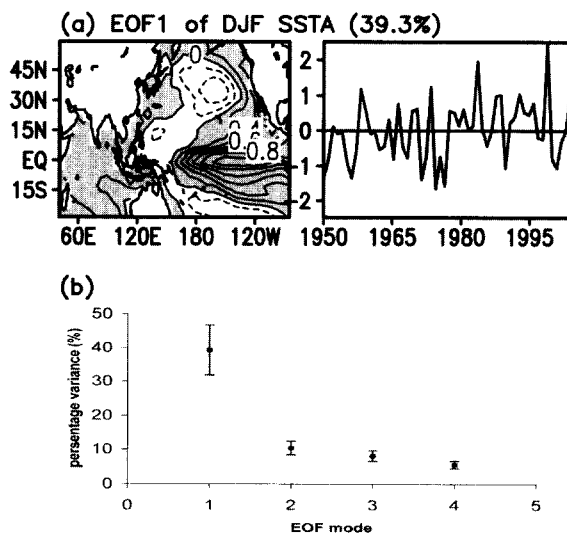


Figure 1. (a) Spatial pattern of the first EOF mode associated with boreal winter (DJF) SST anomalies in the Indo-Pacific Oceans and the corresponding principal component, and (b) percentage variance (%) explained by the first four EOF modes. The error bars represent one standard deviation of the sampling errors [North et al., 1982].

spring and fall seasonal mean, respectively. A covariance matrix is constructed by treating the SSTA in the given seasonal sequence as one time step for the year 0. The derived spatial pattern for each S-EOF mode will contain four sequential patterns representing seasonal evolution of the SSTA. The four-season sequential patterns share the same yearly value in their corresponding PC.

[7] The ratio of the variance associated with a single EOF mode to the total variance defines the variance fraction. Assume that $E_i(\vec{x})$ denotes the spatial pattern of the i th S-EOF mode and T_i the corresponding PC, the fractional variance of the i th mode is defined by the ratio of $E_i(\vec{x})$ multiplied by $\langle T_i(t) \bullet T_i(t) \rangle$ to the total variance of the corresponding seasonal mean SSTA at each grid point, where ' $\langle \rangle$ ' means the variance of a given time series. The geographic distribution of the variance fraction provides information about contributions of a specific

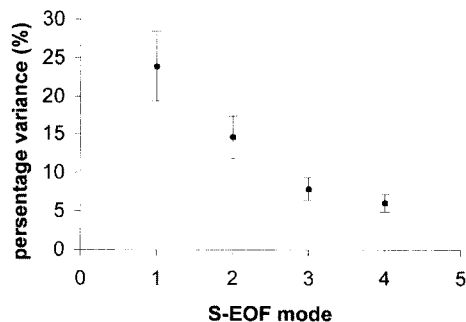


Figure 2. Percentage variance (%) explained by the first four S-EOF modes. The error bars represent one standard deviation of the sampling errors.

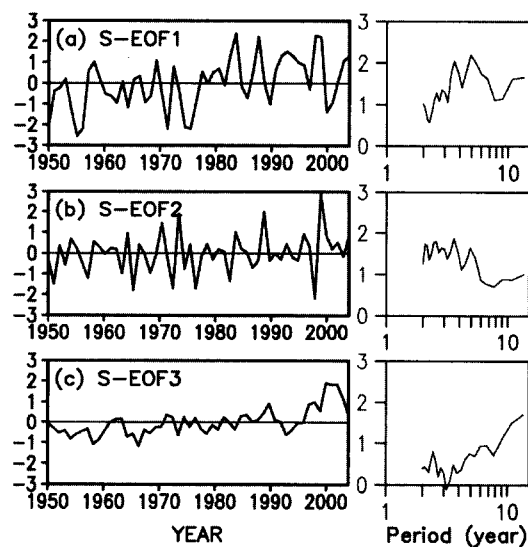


Figure 3. (a) Principal component of the first S-EOF mode of (DJF to SON) SSTA over the Indo-Pacific Ocean and its power spectrum density. (b) and (c) The same as Figure 3a except for the second and third S-EOF modes, respectively.

S-EOF mode to the total variance at a specific location. In S-EOF analysis the variance fraction also varies with season.

[8] The S-EOF analysis was applied to identify major modes of year-to-year SST variability from D(-1)JF(0) to SON(0) in the Indo-Pacific Ocean between 30°S and 60°N. The SST data used are derived from Reynolds [Reynolds and Smith, 1994], which cover the period from 1950 to 2003. The rule of thumb of North et al. [1982] for estimating the sampling error is used to identify statistically significant modes.

3. Distinctions of SSTAs Associated With LF-ENSO and QB-ENSO

[9] Figure 2 shows the variance fraction (percentage) of the first four eigenvalues and the associated unit standard deviation of the sampling errors. According to the rule of North et al., the first two leading modes, which account for 23.9% and 14.6% of the total variance respectively, are well distinguished from each other and from the rest of the EOFs in terms of the sampling error bars. Thus, the first two S-EOF modes are both statistically significant modes.

[10] Figure 3 presents the time series and corresponding spectral densities of the PC1 and PC2. The PC1 reflects all El Niño and La Niña events and has a major spectral peak on 4–6 years (Figure 3a). This mode resembles the LF component of the ENSO identified by Barnett [1991]. For simplicity, we refer the S-EOF 1 to as the LF-ENSO mode. The PC2 shows a biennial variability with a broad spectral peak on 2–3 years (Figure 3b). The biennial oscillation is particularly regular between 1962 and 1977. After the late 1970s, the biennial tendency is mainly associated with the turnabouts of El Niño/La Niña events. This mode resembles the QB component of ENSO [Barnett, 1991]. Its spatial pattern is also similar to the SST variations that are associated with the dominant Asian-Australian monsoon

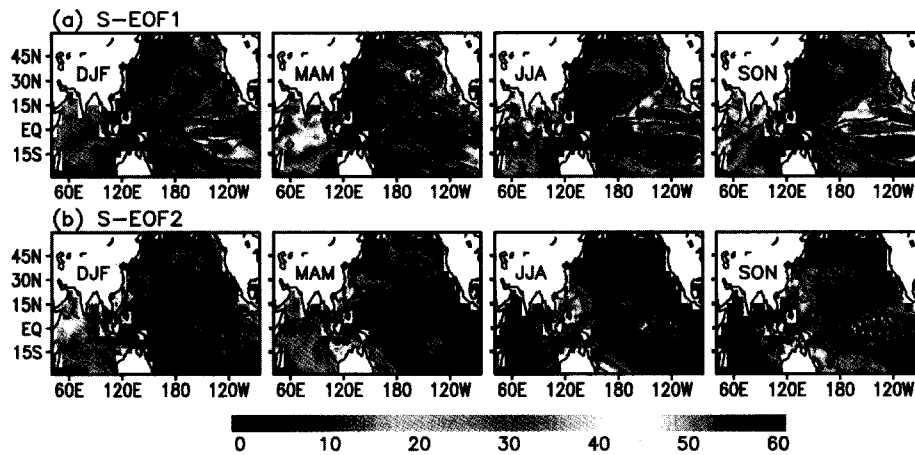


Figure 4. (a) Spatial patterns of the first S-EOF mode of (DJF to SON) SSTA (contours) and the percent variance fraction (color shadings). (b) As in Figure 4a except for the second S-EOF mode. The solid contours starting from 0.1 denote positive values, while the dashed contours starting from -0.1 denote negative values. The contour interval is 0.1.

mode identified by Wang *et al.* [2003], which has a prominent biennial tendency. We refer the S-EOF 2 to as QB-ENSO.

[11] The LF-ENSO and QB-ENSO modes distinguish from each other not only by their dominant periodicity but also by their seasonal evolution, spatial distribution of variance fraction, and the interdecadal variations/long-term trend of their PCs. The seasonal evolutions of spatial patterns of the S-EOF 1 & 2 modes are shown by the contours in Figure 4. In general, the LF-ENSO mode does not vary with season appreciably [e.g., Kim, 2002] (Figure 4a). A region of equatorially symmetric, positive SSTA dominates in the equatorial eastern Pacific. The meridional extent of the warm anomalies increases toward the eastern boundary of the Pacific. The SSTA in the extratropical North Pacific bears close similarity with the SSTA pattern that is driven by ENSO through atmospheric teleconnection [e.g., An and Wang, 2005]. In the equatorial eastern-central Pacific, local westward propagation of the maximum SSTA is discernible throughout the seasonal cycle, which concurs with the canonical scenario described by Rasmusson and Carpenter [1982]. In sharp contrast, the QB-ENSO mode shows a remarkable reversal of SST anomalies in the equatorial eastern-central Pacific from boreal spring to summer (Figure 4b). The SSTA in the eastern Pacific is narrowly trapped to the equatorial region compared with the LF-ENSO mode [e.g., Kim, 2002]. In the Indian Ocean, the seasonal behavior features a rapid development of the Indian Ocean dipole [Saji *et al.*, 1999] or zonal [Webster *et al.*, 1999] mode from boreal summer to fall. After the eastern Indian Ocean warming reaches its maximum in fall, the dipole pattern rapidly decays and changes into a uniform pattern that persists from DJF to the following JJA as discussed by An [2004]. Significant seasonal evolution of the QB-ENSO is also found in the North Pacific. The SSTA appears to be generated during DJF from the western North Pacific and propagates across the basin toward northeast Pacific. The amplitude variation is not linearly proportional to the variation in the tropical ocean, suggesting that the local air-sea interaction or non-linear teleconnection process [Hoerling *et al.*, 1997] may be

important. While the QB-ENSO mode shows eminent seasonal evolution in the eastern-central Pacific and Indian Ocean, it does not show significant seasonal dependence in the maritime continent and the horseshoe region extending from the maritime continent to the subtropical North and South Pacific (Figure 4b). The QB-ENSO in the SSTA of equatorial Indo-Pacific is essentially a standing oscillation.

[12] The geographic distributions of the variance fraction explained by LF-ENSO and QB-ENSO modes are complementary as shown by the color shading in Figure 4. The LF-ENSO mode accounts for over 50% of the total variance in the equatorial Pacific cold tongue and over 40% over the equatorial-North Indian Ocean. Note that the fractional variance on the equator is smaller than that on the off-equatorial regions during JJA and SON. In the extratropical North Pacific, only a small portion of the SST variability ($\sim 20\%$) is explained except during MAM. In contrast, the largest fractional variance carried by the QB-ENSO mode is primarily located in the maritime continent and the associated horseshoe region where the LF-ENSO mode accounts for a smaller proportion (Figure 4b). During JJA and SON, the QB-ENSO mode explains more than 40% of the total variance in the eastern equatorial Pacific and Philippine Sea. In the North Pacific the QB-ENSO also accounts for a significant portion of the total variance (30%).

[13] A notable stepwise rise in the PC1 is observed around 1977, suggesting that the ENSO cycles had experienced a sudden change in the mean state. The interdecadal change of ENSO is reflected not only in its propagation, periodicity, and amplitude [Wang, 1995; An and Wang, 2000], but also in a “jump” of mean state upon which ENSO evolves [Fedorov and Philander, 2000; An and Jin, 2004]. The warm and cold phases prior to and after the climate transition in late-1970s share common spatial patterns with the LF-ENSO mode, suggesting that, this climate transition may be viewed as an ENSO-like interdecadal regime shift [Zhang *et al.*, 1997].

[14] On the other hand, the PC2 of the QB-ENSO mode shows a long-term warming trend that has accelerated since the late 1970s concurring with the global warming

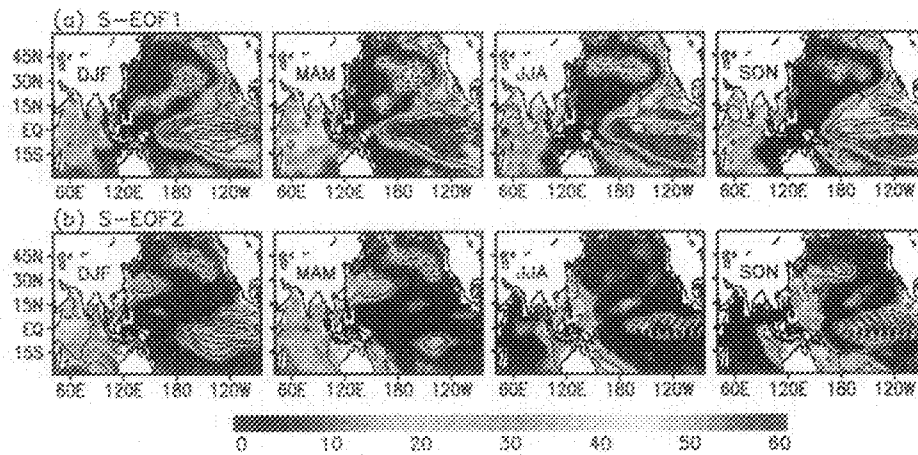


Figure 4. (a) Spatial patterns of the first S-EOF mode of (DJF to SON) SSTA (contours) and the percent variance fraction (color shadings). (b) As in Figure 4a except for the second S-EOF mode. The solid contours starting from 0.1 denote positive values, while the dashed contours starting from -0.1 denote negative values. The contour interval is 0.1.

mode identified by Wang *et al.* [2003], which has a prominent biennial tendency. We refer the S-EOF 2 to as QB-ENSO.

[11] The LF-ENSO and QB-ENSO modes distinguish from each other not only by their dominant periodicity but also by their seasonal evolution, spatial distribution of variance fraction, and the interdecadal variations/long-term trend of their PCs. The seasonal evolutions of spatial patterns of the S-EOF 1 & 2 modes are shown by the contours in Figure 4. In general, the LF-ENSO mode does not vary with season appreciably [e.g., Kim, 2002] (Figure 4a). A region of equatorially symmetric, positive SSTA dominates in the equatorial eastern Pacific. The meridional extent of the warm anomalies increases toward the eastern boundary of the Pacific. The SSTA in the extratropical North Pacific bears close similarity with the SSTA pattern that is driven by ENSO through atmospheric teleconnection [e.g., An and Wang, 2005]. In the equatorial eastern-central Pacific, local westward propagation of the maximum SSTA is discernible throughout the seasonal cycle, which concurs with the canonical scenario described by Rasmusson and Carpenter [1982]. In sharp contrast, the QB-ENSO mode shows a remarkable reversal of SST anomalies in the equatorial eastern-central Pacific from boreal spring to summer (Figure 4b). The SSTA in the eastern Pacific is narrowly trapped to the equatorial region compared with the LF-ENSO mode [e.g., Kim, 2002]. In the Indian Ocean, the seasonal behavior features a rapid development of the Indian Ocean dipole [Saji *et al.*, 1999] or zonal [Webster *et al.*, 1999] mode from boreal summer to fall. After the eastern Indian Ocean warming reaches its maximum in fall, the dipole pattern rapidly decays and changes into a uniform pattern that persists from DJF to the following JJA as discussed by An [2004]. Significant seasonal evolution of the QB-ENSO is also found in the North Pacific. The SSTA appears to be generated during DJF from the western North Pacific and propagates across the basin toward northeast Pacific. The amplitude variation is not linearly proportional to the variation in the tropical ocean, suggesting that the local air-sea interaction or non-linear teleconnection process [Hoerling *et al.*, 1997] may be

important. While the QB-ENSO mode shows eminent seasonal evolution in the eastern-central Pacific and Indian Ocean, it does not show significant seasonal dependence in the maritime continent and the horseshoe region extending from the maritime continent to the subtropical North and South Pacific (Figure 4b). The QB-ENSO in the SSTA of equatorial Indo-Pacific is essentially a standing oscillation.

[12] The geographic distributions of the variance fraction explained by LF-ENSO and QB-ENSO modes are complementary as shown by the color shading in Figure 4. The LF-ENSO mode accounts for over 50% of the total variance in the equatorial Pacific cold tongue and over 40% over the equatorial-North Indian Ocean. Note that the fractional variance on the equator is smaller than that on the off-equatorial regions during JJA and SON. In the extratropical North Pacific, only a small portion of the SST variability ($\sim 20\%$) is explained except during MAM. In contrast, the largest fractional variance carried by the QB-ENSO mode is primarily located in the maritime continent and the associated horseshoe region where the LF-ENSO mode accounts for a smaller proportion (Figure 4b). During JJA and SON, the QB-ENSO mode explains more than 40% of the total variance in the eastern equatorial Pacific and Philippine Sea. In the North Pacific the QB-ENSO also accounts for a significant portion of the total variance (30%).

[13] A notable stepwise rise in the PC1 is observed around 1977, suggesting that the ENSO cycles had experienced a sudden change in the mean state. The interdecadal change of ENSO is reflected not only in its propagation, periodicity, and amplitude [Wang, 1995; An and Wang, 2000], but also in a "jump" of mean state upon which ENSO evolves [Fedorov and Philander, 2000; An and Jin, 2004]. The warm and cold phases prior to and after the climate transition in late-1970s share common spatial patterns with the LF-ENSO mode, suggesting that this climate transition may be viewed as an ENSO-like interdecadal regime shift [Zhang *et al.*, 1997].

[14] On the other hand, the PC2 of the QB-ENSO mode shows a long-term warming trend that has accelerated since the late 1970s concurring with the global warming

(Figure 3b). Since the QB-ENSO mode accounts for a major portion of the local SST variability over the Maritime Continent-western Pacific horseshoe region where the QB-ENSO shows little seasonal-dependence, the warming trend of the PC2 implies that a persistent warming trend that accounts for a large portion of the local SST variability exists in the Maritime Continent-western Pacific horseshoe region.

4. Discussion

[15] The 3rd S-EOF mode represents a quasi-annual mode that is a narrowly trapped equatorial mode propagating westward from South American coast in northern spring to the central Pacific in fall-winter (figure not shown). Although this mode is not statistically distinguishable from the 4th mode over the entire analysis period, it becomes noteworthy in the recent years after 1997 (Figure 3c). The intensification of the quasi-annual mode in recent years may be related to the extended cold state of the tropical Pacific after the 1997/98 El Niño event, which provides a favorable condition for such a fast mode because of the increase in the background zonal SST gradient [Jin *et al.*, 2003]. The Pacific Decadal Oscillation [Mantua *et al.*, 1997] appears as the 4th S-EOF mode (figure not shown), which is not significantly distinguished from other modes. Thus, the SST variability beyond ENSO time scale appears to be primarily represented by the ENSO like interdecadal regime shift occurred in the late 1970s.

[16] The S-EOF is, to some extent, similar to that of extended EOF analysis [Weare and Nasstrom, 1982] except that the S-EOF deals with a season-dependent evolution with reference to the annual cycle, not an arbitrary four-season sequence, which can start from any individual season. For instance, when the covariance matrix for the eigenvalue analysis is XX^T , where \vec{x} is a spatial state vector, the matrix for the S-EOF is $X(\vec{x}, t) = [\vec{x}^{DJF}(t), \vec{x}^{MAM}(t), \vec{x}^{JJA}(t), \vec{x}^{SON}(t)]$, where $t = \text{year}$, while the matrix for the extended EOF is $X(\vec{x}, t) = [\vec{x}(t), \vec{x}(t+1), \vec{x}(t+2), \vec{x}(t+3)]$, where $t = \text{season}$. In the latter, the derived EOFs would smear the effects of annual cycles on the interannual variability and fail to distinguish the LF- and QB-ENSOS. The 'periodically extended EOF technique' by Kim and Wu [1999] may be more close to the S-EOF. However, it was applied in a different manner. Kim [2002] and Kim *et al.* [2003] also identified the LF and QB modes using the Cyclostationary EOF (CSEOF). Different from the S-EOF that relies on neither pre-assumed periodicity nor pre-filtering of the data, the CSEOF of ENSO anomalies relies on a pre-assumed 2-year (imbedded) periodic variability.

[17] The S-EOF analysis may be sensitive to the choice of seasonal sequence. If a seasonal sequence starting from JJA(0) to MAM(1) were used, the QB-ENSO mode identified in this study would no longer exist. The reason is that the phase transition of QB-ENSO occurs between MAM and JJA and the extreme polarity in SSTA exists during DJF and SON. Thus, the seasonal sequence from DJF to SON maximizes the QB-ENSO signal. In general, physical con-

sideration is of importance in application of the S-EOF analysis.

[18] **Acknowledgments.** This study is supported by NOAA OGP through Pacific Program and by the Japan Agency for Marine-Earth Science and Technology through its sponsorship of the International Pacific Research Center. SOEST number 6627 and IPRC number 341.

References

- An, S.-I. (2004), A dynamic link between the basin-scale and zonal modes in the tropical Indian Ocean, *Theor. Appl. Climatol.*, **78**, 203–215.
- An, S.-I., and F.-F. Jin (2004), Nonlinearity and asymmetry of ENSO, *J. Clim.*, **17**, 2399–2412.
- An, S.-I., and B. Wang (2000), Interdecadal change of the structure of the ENSO mode and its impact on the ENSO frequency, *J. Clim.*, **13**, 2044–2055.
- An, S.-I., and B. Wang (2001), Mechanisms of locking of the El Niño and La Niña mature phase to boreal winter, *J. Clim.*, **14**, 2164–2176.
- An, S.-I., and B. Wang (2005), The forced and intrinsic low-frequency modes in the North Pacific, *J. Clim.*, **18**, 876–885.
- Barnett, T. P. (1991), The interaction of multiple time scales in the tropical climate system, *J. Clim.*, **4**, 269–285.
- Fedorov, A. V., and S. G. Philander (2000), Is El Niño changing?, *Science*, **288**, 1997–2002.
- Hoerling, M. P., A. Kumar, and M. Zhong (1997), El Niño, La Niña, and the nonlinearity of their teleconnections, *J. Clim.*, **10**, 1769–1786.
- Jin, F.-F., J.-S. Kug, S.-I. An, and I.-S. Kang (2003), A near-annual coupled ocean-atmosphere mode in the equatorial Pacific Ocean, *Geophys. Res. Lett.*, **30**(2), 1080, doi:10.1029/2002GL015983.
- Kim, K.-Y. (2002), Investigation of ENSO variability using cyclostationary EOFs of observational data, *Meteorol. Atmos. Phys.*, **81**, 149–168.
- Kim, K.-Y., and Q. Wu (1999), A comparison study of EOF techniques: Analysis of nonstationary data with periodic statistics, *Clim. J.*, **12**, 185–199.
- Kim, K.-Y., J. J. O'Brien, and A. I. Barcilon (2003), The principal physical modes of variability over the tropical Pacific, *Earth Interactions*, **7**(3), 1–32.
- Lorenz, E. N. (1956), Empirical orthogonal functions and statistical weather prediction, *Sci. Rep.*, **1**, 49 pp., Mass. Inst. of Technol., Cambridge.
- Mantua, N. J., S. R. Hare, Y. Zhang, J. M. Wallace, and R. C. Francis (1997), A Pacific decadal climate oscillation with impacts on salmon, *Bull. Am. Meteorol. Soc.*, **78**, 1069–1079.
- North, G. R., T. L. Bell, R. F. Cahalan, and F. J. Moeng (1982), Sampling errors in the estimation of empirical orthogonal functions, *Mon. Weather Rev.*, **110**, 699–706.
- Rasmusson, E. M., and T. H. Carpenter (1982), Variations tropical sea surface temperature and surface wind fields associated with the Southern Oscillation/El Niño, *Mon. Weather Rev.*, **110**, 354–384.
- Reynolds, R. W., and T. M. Smith (1994), Improved global sea surface temperature analysis using optimum interpolation, *J. Clim.*, **7**, 929–948.
- Saji, N. H., B. N. Goswami, P. N. Vinayachandran, and T. Yamagata (1999), A dipole mode in the tropical Indian Ocean, *Nature*, **401**, 360–363.
- Wang, B. (1995), Interdecadal changes in El Niño onset in the last four decades, *J. Clim.*, **8**, 267–285.
- Wang, B., and Z. Fang (1996), Chaotic oscillation of tropical climate: A dynamic system theory for ENSO, *J. Atmos. Sci.*, **53**, 2786–2802.
- Wang, B., R. Wu, and T. Li (2003), Atmosphere-warm ocean interaction and its impact on Asian-Australian monsoon variation, *J. Clim.*, **16**, 1195–1211.
- Weare, B. C. (1982), El Niño and tropical Pacific Ocean surface temperatures, *J. Phys. Oceanogr.*, **12**, 17–27.
- Weare, B. C., and J. S. Nasstrom (1982), Examples of extended empirical orthogonal function analyses, *Mon. Weather Rev.*, **110**, 481–485.
- Webster, P. J., A. M. Moore, J. P. Loschnigg, and R. R. Leben (1999), Coupled ocean-atmosphere dynamics in the Indian Ocean during 1997–98, *Nature*, **401**, 356–360.
- Zhang, Y., J. M. Wallace, and D. S. Battisti (1997), ENSO-like interdecadal variability: 1900–93, *J. Clim.*, **10**, 1004–1020.

S.-I. An and B. Wang, International Pacific Research Center, SOEST, University of Hawaii'i at Manoa, 1680 East-West Road, Honolulu, HI 96822, USA. (sian@hawaii.edu)